Journal of Materials Chemistry C

Accepted Manuscript

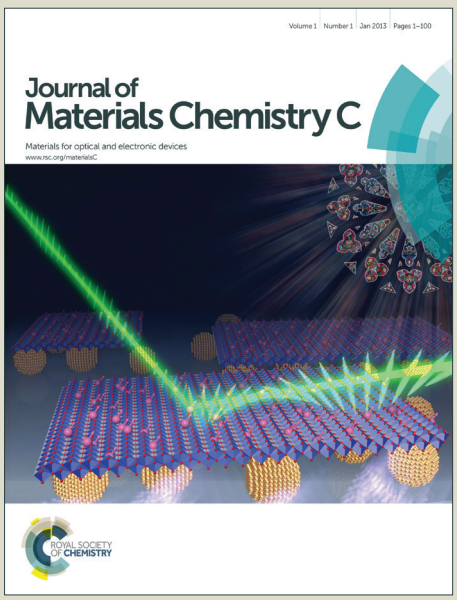

ROYAL SOCIETY OF CHEMISTRY

www.rsc.org/materialsC

Cite this: DOI: 10.1039/c0xx00000x

www.rsc.org/xxxxxx

PAPER

High-performance UV/visible photodetector of Cu_2O/ZnO hybrid nanofilms on SWNTs-based flexible conducting substrates

Xianbin Liu,*[a] Hejun Du,*[a] Penghua Wang,[b] Teik-Thye Lim,[b,c] and Xiao Wei Sun[d]

Received (in XXX, XXX) Xth XXXXXXXXX 20XX, Accepted Xth XXXXXXXXX 20XX

DOI: 10.1039/b000000x

In this report, we present a photosensing unit based on single-walled nanotubes (SWNTs) integrated with Cu_2O/ZnO hybrid nanofilms. 50-nm Cu_2O and 50-nm ZnO nanofilms are respectively deposited on a SWNTs-coated polyethylene terephthalate (PET) sheet via a two-step sputtering process. The Cu_2O/ZnO nanofilm photodetector exhibits rapid response (<100 ms), excellent responsive repeatability, robust stability and broadband photodetection range from 365 to 625 nm without external bias. Furthermore, ZnO/Cu_2O nanofilm photodetector has been also fabricated by changing deposition sequence of ZnO and Cu_2O. The photocurrent of the ZnO/Cu_2O nanofilm photodetector is one-fourth of that of the Cu_2O/ZnO nanofilm photodetector. We speculate that it might be attributed to the presence of the whispering-gallery mode (WGM) resonances in Cu_2O/ZnO hybrid nanofilms owing to the higher refractive index of Cu_2O, resulting in enhancing the light trapping and absorption. The high performance of Cu_2O/ZnO nanofilm photodetector indicates that the Cu_2O/ZnO hybrid nanofilms on SWNTs-based conducting substrates are suitable for mass production and application as high-sensitivity, fast response speed and flexible UV/visible photodetectors.

Introduction

Pure ZnO, with a wide band gap of ~3.37 eV, is only feasible for photodetection in the UV range,[1-5] which restricts its potential applications in photocatalysis, photovoltaics and photosensors with a broad optical spectral sensitivity. Many attempts have been made to introduce intermediate band gap states in ZnO, including doping with carbon,[6-10] sulphur,[11] or nitrogen,[12,13] to extend the optical absorption of ZnO into visible light. However, it requires synthesizing at high temperature, complicated process control, and rigorous conditions.

Cuprous oxide (Cu_2O) is a natural p-type semiconductor and its band gap was reported to be 1.9-2.2 eV,[14-16] which can be photoexicited in UV-visible spectral region. It is one of the most studied metal oxides for solar cells,[17-19] photocatalysts,[20,21] photosensors,[22,23] and photoeletrochemical (PEC) applications,[24-26] because of its high optical absorption coefficient, nontoxicity, abundant availability and low production cost. It is believed that coupling ZnO with Cu_2O can improve the photoresponse of the visible photocatalysis and facilitate the charge separation, and hence enhance the photocatalytic performance.[20] A few studies of ZnO/Cu_2O heterojunction have been reported for photovoltaic,[17] photocatalytic,[20,27] and photosensitive[28,29] applications.

Single-walled carbon nanotubes (SWNTs) have exceptional conductivity, high carrier mobility and high mechanical strength. Consequently, SWNT thin films are explored as an alternative to indium tin oxide (ITO) for electronic and optoelectronic applications.[30,31] Apart from exceptional conductivity, excellent flexibility and optical transparency, SWNT thin films exhibit hollow structure with tube-tube junction, which can improve sensing applications owing to high specific surface area.

In our present work, a flexible photodetector based on Cu_2O/ZnO hybrid nanofilms, was reported for the first time by depositing ZnO and Cu_2O on SWNTs-based PET by a two-step sputtering process. The Cu_2O/ZnO nanofilm photodetector demenstrated fast, reversible and stable photoresponse charateristics under UV/visible illumination without external bias. By changing the deposition order of ZnO and Cu_2O, the ZnO/Cu_2O nanofilm photodetector were fabricated, which also exhibted excellent UV/visible photoresponse. However, it was found that the Cu_2O/ZnO nanofilm photodetector could produce much stronger photocurrent as compared to the ZnO/Cu_2O nanofilm photodetector in the same condition. It can be attributed to forming of the whispering-gallery resonant modes in Cu_2O/ZnO hybrid nanofilms owing to the higher refractive index of Cu_2O, resulting in enhancing the light trapping and absorption, and hence stronger photoresponse was obtained in Cu_2O/ZnO nanofilm photodetector. These results indicate that the Cu_2O/ZnO hybrid nanofilms are highly promising candidates for applications in high-sensitivity, fast response speed and flexible photodetectors with broad band photoresponse.

Experimental section

Preparation and characterization of Cu_2O/ZnO nanofilms on SWNTs-based flexible PET

The SWNTs were dispersed in deionized (DI) water by sonication with the aid of surfactant (1% solution of sodium dodecyl sulfate (1 mg/ml)). Then a piece of PET sheet of 100 μm

thick was processed by oxygen plasma for 20 min. After oxygen plasma surface treatment, the SWNTs dispersion was coated onto the PET sheet with stainless steel rods.

The SWNTs-based PET sheet was then used as the substrates for depositing Cu_2O/ZnO nanofilms by radio-frequency (RF) magnetron sputtering at room temperature. The sputtering was carried out at an RF power of 70 W. The working pressure is 0.8 Pa. ZnO layers were deposited by sputtering ZnO target of 99.99 % purity with 10 standard cubic centimeters per minute (sccm) Ar flow. Cu target of 99.99 % purity, Ar sputtering gas (8 sccm) and O_2 reactive gas (2 sccm) were used for the deposition of Cu_2O layers. The thickness of ZnO and Cu_2O layers were about 50 nm each. Finally, a 20-nm thick ITO conductive layer was deposited as the top electrode using electron beam (E-beam) evaporation.

The surface morphologies of the as-prepared products were characteriazed with a field emission scanning electron microscopy (FESEM, JEOL, JSM-7600F). The crystalline structures of the samples were determined by using a x-ray diffractometer (XRD, PANalytical EMPYREAN). The optical absorption spectra of the films were measured by a UV-Vis spectrophotometer (Shimadzu UV-2450). The chemical composition was analyzed by X-ray photoelectron spectroscopic (XPS, KRATOS, AXIS ULTRA) with a monochromated AlKα (1486.7 eV) X-ray source at a power of 150 W (15 kV × 10 mA). The spectra were corrected by referencing the binding energy to the C1s peak at 284.6 eV.

Electrical and photoelectrical characterization

The measurement of electrical and photoelectric properties of the devices were conducted using a CHI 760 electrochemical workstation with two-electrode configuration by short-circuiting the auxiliary and reference electrodes together. High quality 5050 single color SMD LEDs were used as light source. For each color of LED lights, one-meter LED strip (60 units) was cut into 10 pieces and parallelled together on a flat panel (10 cm × 10 cm). The light intensity of the homemade LED light panels were characterized by Pyranometer CMP6 (Kipp & Zonen) at a special distance between the light and the device (See Table S1).

Results and discussion

Fig. 1a and d show the low and high magnified SEM images of the SWNTs-coated PET sheet. As the carbon nanotube dispersion was coated on the PET sheet, the nanotubes were intertwined together to form a network, as clearly seen from the magnified image (Fig. 1c). As carbon nanotubes are conductive, it is indicated that a conductive 2D network was formed on the flexible PET sheet. The sheet resistance is 20-200 kΩ/square and its transmittance is about 95%.[30,32] After 50-nm ZnO deposition, the carbon nanotubes were covered with ZnO nanocrystallines, resulting in formation of the ZnO/SWNTs hybrid nanofilms (Fig. 1b and e). From the enlarged SEM image in Fig. 1e, the ZnO nanocrystallines are with sizes of 20-30 nm. Before depositing Cu_2O, it can be clearly seen that there were many gaps existed in the ZnO/SWNTs hybrid nanofilms. However, after 50-nm Cu_2O deposition, no much grid mesh was left and the net wires became much thicker (Fig. 1c and f). As shown in Fig. 1f, the Cu_2O nanocrystallines were with sizes of 20-30 nm. It is expected that the absorption edge of Cu_2O is about 2.04 eV as equal to that of bulk Cu_2O when the nanoparticle size is larger than 20 nm.[33] The optical absorption edge of 2.04 eV indicates that Cu_2O can be well excited in the visible light (<600 nm). Fig. 1g depicts the optical image of the flexible PET sheet with Cu_2O/ZnO/SWNTs nanofilms. As introduced in experimental part, the PET sheet was treated by oxygen plasma before coating carbon nanotube film on it. It is believed that oxygen plasma surface treatment can assist in creating chemically active functional groups, such as amine, carbonyl, hydroxyl and carboxyl groups, to improve interfacial adhesion of PET with carbon nanotubes. Moreover, carbon nanotubes are inherently flexible, strong, and chemically resistant. After depositing Cu_2O/ZnO layers, the change of the SWNTs network is insignificant. Therefore, the Cu_2O/ZnO/SWNTs nanofilms are mechanical flexible and robust.

XRD measurements were conducted to investigate the compostion of the resultant samples as shown in Fig. 2. The diffraction peaks at 2θ ~25.9º are attributed to the PET substrate. It is known that the charateristic peak of SWNTs is around 43.42º and indexed (100), originating from the graphene nature of SWNTs.[34] As shown in Fig. 2b, a weak peak around 43º can be identified in SWNTs-coated PET sheet, indicating the exsistance of SWNTs. After dopesiting ZnO on SWNTs-coated PET, the peak of ZnO (002) can be observed at ~34.2º as displayed in Fig. 2c. After Cu_2O depostion, as shown in Fig. 2d, the diffraction peaks at 36.5º and 42.6º were observed, which can be assigned to the (111) and (200) planes of Cu_2O.[20,22]

The XPS measurement was carried out to evaluate the surface compositions of the samples. A typical XPS survey spectrum demonstrates the existence of Cu, Zn, O and C in the Cu_2O/ZnO/SWNTs nanofilms, as shown in Fig. 3a. The Cu 2p XPS spectrum presented in Fig. 3b shows the peaks of Cu $2p_{3/2}$ and Cu $2p_{1/2}$ are located at 932.7 and 952.6 eV, respectively, which can be assigned as the contributions of the monovalence copper.[20,22,23] That result indicates Cu 2p in Cu_2O phase. Meanwhile, the peaks of Cu 2p at 961.2 and 942.7 eV were observed, indicating the slight oxidation of some Cu(I) ions on the surface layer of the Cu_2O nanoparticles as the previous reports.[22,23] Fig. 3c displays Zn 2p3/2 and Zn 2p1/2 states with the binding energies aound 1020.5 and 1043.6 eV, respectively, which is assigned to the Zn^{2+} in ZnO. The peak of O 1s shown in Fig. 3d indicates O is contributed from Cu_2O and ZnO layers.

The Cu_2O/ZnO hybrid nanofilms were prepared on SWNTs-based PET via two-step RF magnetron sputtering, as demonstrated in Fig. 4a. A 50-nm ZnO layer (yellow) was first deposited on SWNTs-based PET, and the carbon nanotubes (black) was covered with ZnO. Then, a 50-nm Cu_2O (orange) layer was deposited in sequence, and the ZnO/Cu_2O hybrid nanofilms were fabricated on SWNTs-based PET. Followed ITO (transparent) deposition using E-beam evaporation, that is, a photon sensitive device with ITO/Cu_2O/ZnO/SWNTs structure was built with the SWNTs network as source electrode and ITO layer as drain electrode. Silver pastes were then used to connect the two electrodes with the external circuits.

Fig. 4b shows the current–voltage (I-V) characteristics of the Cu_2O/ZnO photodetector under dark condition. It is noted that the I-V curve is quasi-symmetric with an inferior rectification characteristic. As the negative bias was increased, the leakage current was increased as well, indicating the existence of

interfacial defects in the Cu_2O/ZnO hybrid nanofilm.[23,35] The quasi-symmetric behavior[36] demonstrates unrestricted free carriers transfer at the Cu_2O/ZnO interface.

To test the photoresponse of the Cu_2O/ZnO hybrid nanofilms for UV-visible spectral region, four types of monochromic LEDs, were used as light sources, spectral peaks at 365, 425, 525 and 625 nm, respectively. Without applied bias, as shown in Fig. 4c, the typical photocurrents can be generated under UV and visible illuminations, indicating that the device can be operated as a photovoltaic cell and no external power needed for photoreponse. It is noted that the Cu_2O/ZnO photodetector can produce very stable photocurrent, indicating excellent photoresponsive reversibility and stability. Fig. 4d presents the photocurrent transient measurement by periodically switching on and off the white LED lights with different power intensities in the absence of external bias. It can be seen that the photoresponsivity, defined as the ratio of the current under the illumination to that under the dark, can reach 520, which is a significant increase of 3000% compared to the result presented in a recent report.[37] Along with the increase of light power intensities, the photocurrents were increased as well, and the photocurrent is linearly proportional to the light intensity ($I=4.54P + 2.03$, where I is photocurrent, and P is the light power intensity) as indicated in Fig. S1. This indicates that the enhanced photogenerated electron-hole pairs can be efficiently separated at the interface of the Cu_2O/ZnO hybrid nanofilms, which is a significant mechanism for achieving high sensitivity and quick response for the photodetectors. Fig. 4e shows the photoresponse dynamics, the rising and decaying rates of the photocurrent are pretty rapid, and faster than the limit of the present measurement setup (100 ms). This photoresponse is faster than that of most other photodetectors.[4,8,10,28,29]

Furthermore, a comparison experiment was carried out via switching ZnO and Cu_2O deposition order on SWNTs-based PET. Then an ITO layer was deposited as drain electrode, i.e., ITO/ZnO/Cu_2O/SWNTs structure was built for photosensitive detection as shown in Fig. 5a. In the same testing conditions, as displayed in Fig. 5b, c, it is interesting to find that the photocurrents of the ZnO/Cu_2O nanofilm photodetectors were minus and opposite to that of the Cu_2O/ZnO nanofilm photodetector. The charge transfer and transport process in the hybrid nanofilms can be understood from the energy level diagrams as illustrated in Fig. 6a, b, based on the published values of conduction band (CB) edge and valence band (VB) edge positions for SWNTs,[38,39] ZnO,[10,40] Cu_2O,[41,42] and ITO.[43] For the Cu_2O/ZnO hybrid nanofilms, p-n junction formed at their interface and the band alignment could facilitate the electron transport from the conduction band of Cu_2O to the conduction band of ZnO.[23,27] So it is easy to understand that the photocurrents of the photodetectos with ITO/Cu_2O/ZnO/SWNTs structure was totally opposite to that of the photodetectos with ITO/ZnO/Cu_2O/SWNTs structure. Apart from generating opposite photocurrents, illuminating the devices upon various LED lights without applied bias, as shown in Fig. 4c, d, and Fig. 5b, c, both ZnO/Cu_2O and Cu_2O/ZnO nanofilm photodetectors demonstrate fast, reversible and stable photoresponse charateristics under the UV/visible illumination. Moreover, as shown in Fig. S1, the photocurrent in the ZnO/Cu_2O nanofilm photodetectors is almost linearly proportional to the light intensity upon the white LED irradiation as well. The relationship of the photocurrent vs. the light intensity can be expressed as for ZnO/Cu_2O: $I=1.21P-0.57$; whilst for Cu_2O/ZnO: $I=4.54P + 2.03$, where I is photocurrent, and P is the light power intensity. The linear slope can reflect the photoresponsivity to a certain extent. That is, the photoresponse of the Cu_2O/ZnO nanofilm devices is much stronger than that of the ZnO/Cu_2O nanofilm devices.

In addition, the photoresponse performance of the ZnO/Cu_2O nanofilm photodetector was inferior to that of the Cu_2O/ZnO nanofilm photodetector, although it was much stronger than that of the Cu_2O nanofilm photodetector (see Fig. S1). The photocurrent of the Cu_2O/ZnO photodetector is almost four-fold of that of the Cu_2O/ZnO photodetector under irradiation at the same intensity. For example, under white LED irradiation at the light intensity of 28.7 mW/cm^2, the ZnO/Cu_2O nanofilm photodetectors can only produce photocurrents of 35.10 nA as shown in Fig. 5c, compared to that of the Cu_2O/ZnO photodetector 131.86 nA (Fig. 4d). Only changing the deposit order of ZnO and Cu_2O, the photoresponse exhibited such obvious differences. Regarding to the effect of the deposition sequences of ZnO and Cu_2O, one similar finding has been reported by Akimoto at el.[15] suggesting that the devices with Cu_2O deposited on ZnO was expected to have the similarity of the atomic arrangement and lower defect densities in the interface between ZnO and Cu_2O. Recently, it is reported that embedding low-index absorptive inclusions in a high-index medium can significantly enhance light absorption beyond the upper limit of $4n^2/\sin^2\theta$, where n is the refractive index, and θ the angle of the emission cone in the medium surrounding the cell.[44] The refractive index of Cu_2O prepared by reactive sputtering is 2.8-3.4 in the visible range,[45] while ZnO has a lower refractive index (n=2.0-2.4).[46] As shown in Fig. 4a, the low-index absorptive ZnO was included in the high-index Cu_2O, so the light absorption of the Cu_2O/ZnO hybrid nanofilms would be remarkably enhanced, resulting in stronger photoresponse. Furthermore, such phenomena can be also attributed to the presence of whispering gallery mode (WGM) resonances.[47,48] When a higher refractive index shell layer is located on a lower refractive index core layer (i.e., ZnS/ZnO[47]), the WGM resonances will appear in the active shell layer, which can dramatically reinforce the light trapping and absorption. Herein, ZnO, Cu_2O, ZnO/Cu_2O and Cu_2O/ZnO nanofilms were prepared on transparent glass slide and UV-vis absorption spectra were measured ranging from 300 to 800 nm as shown in Fig. 6c. It can be clearly seen that Cu_2O/ZnO nanofilm has strongest optical absorption in the four kinds of nanofilms, further experimentally confirming that as the Cu_2O layer (external shell) is placed upon the ZnO layer (internal shell), the light trapping of absorption in the Cu_2O/ZnO nanofilm can be enhanced dramatically. Therefore, it is understood that the optical absorption and the photocurrent in the Cu_2O/ZnO nanofilm are much stronger than that in the ZnO/Cu_2O nanofilm.

Conclusions

In conclusion, Cu_2O/ZnO hybrid nanofilms were synthesized on SWNTs-based flexible conducting PET sheet by a simple two-step RF sputtering deposition. The obtained Cu_2O/ZnO hybrid nanofilms exhibited fast response (<100 ms), excellent responsive repeatability, robust stability and broadband photodetection range

from 365 to 625 nm. Meanwhile, by changing deposition sequence of ZnO and Cu_2O, the ZnO/Cu_2O nanofilm photodetectors were fabricated, which also demenstrated fast, reversible and stable photoresponse charateristics under the UV/visible illumination. However, the photocurrent of the ZnO/Cu_2O nanofilms was inferior to that of the Cu_2O/ZnO nanofilms under the same irradiation. It can be attributed to the appearance of the WGM resonances due to the higher refractive index of Cu_2O (external shell) in Cu_2O/ZnO hybrid thin films, resulting in the enhancement of the light trapping of absorption. This present work provides a simple feasible and reproducible mehtod for fabricating high-performance flexible UV/visble photodetectors without power consumption.

Notes and references

[a] *School of Mechanical and Aerospace Engineering, Nanyang Technological University, Singapore. Fax: +65 6795 4630; Tel: +65 6795 4783; E-mail: liuxianbin@ntu.edu.sg, and mhdu@ntu.edu.sg*
[b] *Nanyang Environment and Water Research Institute (NEWRI), Nanyang Technological University, Singapore*
[c] *School of Civil and Environmental Engineering, Nanyang Technological University, Singapore*
[d] *School of Electrical and Electronic Engineering, Nanyang Technological University, Singapore*

1 K. Liu, M. Sakurai and M. Aono, *Sensors*, 2010, **10**, 8604-8634.
2 H. Kind, H. Yan, B. Messer, M. Law and P. Yang, *Adv. Mater.*, 2002, **14**, 158.
3 T. Y. Zhai, X. S. Fang, M. Y. Liao, X. J. Xu, H. B. Zeng, B. Yoshio and D. Golberg, *Sensors*, 2009, **9**, 6504-6529.
4 M. Chen, L. Hu, J. X. Xu, M. Y. Liao, L. M. Wu and X. S. Fang, *Small*, 2011, **7**, 2449-2453.
5 L. L. Shi, F. Wang, B. H. Li, X. Chen, B. Yao, D. X. Zhao and D. Z. Shen, *J. Mater. Chem. C*, 2014, **2**, 5005-5010.
6 X. B. Liu, H. J. Du and X. W. Sun, *RSC Adv.*, 2014, **4**, 5136-5140.
7 S. Cho, J. W. Jang, J. S. Lee and K. H. Lee, *CrystEngComm*, 2010, **12**, 3929-3935.
8 X. B. Liu, H. J. Du, X. W. Sun, B. Liu, D. W. Zhao and H. D. Sun, *CrystEngComm*, 2012, **14**, 2886-2890.
9 S. W. Liu, C. Li, J. G. Yu and Q. J. Xiang, *CrystEngComm*, 2011, **13**, 2533-2541.
10 X. B. Liu, H. J. Du, X. W. Sun, Z. Y. Zhan, G. Z. Sun, F. J. Li, L. X. Zheng and S. Zhang, *J. Nanosci.Nanotechnol.*, 2014, **14**, 7066-7071.
11 C. Kim, S. J. Doh, S. G. Lee, S. J. Lee and H. Y. Kim, *Appl. Catal. A: Gen.*, 2007, **330**, 127-133.
12 X. Y. Yang, A. Wolcott, G. M. Wang, A. Sobo, R. C. Fitzmorris, F. Qian, J. Z. Zhang and Y. Li, *Nano Lett.*, 2009, **9**, 2331-2336.
13 X. Zong, C. Sun, H. Yu, Z. G. Chen, Z. Xing, D. Ye, G. Q. Lu, X. Li and L. Wang, *J. Phys. Chem. C*, 2013, **117**, 4937-4942.
14 P. E. de Jongh, D. Vanmaekelbergh and J. J. Kelly, *Chem. Commun.*, 1999, 1069-1070.
15 K. Akimoto, S. Ishizuka, M. Yanagita, Y. Nawa, G. K. Paul and T. Sakurai, *Sol. Energy*, 2006, **80**, 715-722.
16 T. Jiang, T. Xie, Y. Zhang, L. Chen, L. Peng, H. Li and D. Wang, *Phys. Chem. Chem. Phys.*, 2010, **12**, 15476-15481.
17 T. Minami, Y. Nishi, T. Miyata and J. I. Nomoto, *Appl. Phys. Express*, 2011, **4**, 062301.
18 J. Cui and U. J. Gibson, *J. Phys. Chem. C*, 2010, **114**, 6408-6412.
19 M. Izaki, T. Shinagawa, K. T. Mizuno, Y. Ida, M. Inaba and A. Tasaka, *J. Phys. D: Appl. Phys.*, 2007, **40**, 3326.
20 X. Zou, H. Fan, Y. Tian and S. Yan, *CrystEngComm*, 2014, **16**, 1149-1156.
21 H. Xu, W. Wang and W. Zhu, *J. Phys. Chem. B*, 2006, **110**, 13829-13834.
22 J. Xu, Y. Cao, J. Wei, J. L. Sun, J. Xu and J. He, *Mater. Res. Express*, 2014, **1**, 015002.
23 M. Yang, J. Xu, J. Wei, J. L. Sun, W. Liu and J. L. Zhu, *Appl. Phys. Lett.*, 2012, **100**, 253113.
24 Y. Mao, J. He, X. Sun, W. Li, X. Lu, J. Gan, Z. Liu, L. Gong, J. Chen and P. Liu, *Electrochim. Acta*, 2012, **62**, 1-7.
25 P. Wang, Y. H. Ng and R. Amal, *Nanoscale*, 2013, **5**, 2952-2958.
26 M. Hara, T. Kondo, M. Komoda, S. Ikeda, K. Shinohar, A. Tanaka, J. N. Kondoa and K. Domen, *Chem. Commun.*, 1998, 357-358.
27 M. Deo, D. Shinde, A. Yengantiwar, J. Jog, B. Hannoyer, X. Sauvage, M. More and S. Ogale, *J. Mater. Chem.*, 2012, **22**, 17055-17062.
28 R. C. Wang and H. Y. Lin, *Sensor. Actuat. B: Chem.*, 2010, **149**, 94-97.
29 M. Deo, S. Mujawar, O. Game, A. Yengantiwar, A. Banpurkar, S. Kulkarni, J. Jog and S. Ogale, *Nanoscale*, 2011, **3**, 4706-4712.
30 H. Z. Geng, K. K. Kim, K. P. So, Y. S. Lee, Y. Chang and Y. H. Lee, *J. Am. Chem. Soc.*, 2007, **129**, 7758-7759.
31 J. Li, L. Hu, L. Wang, Y. Zhou, G. Grüner and T. J. Marks, *Nano Lett.*, 2006, **6**, 2472-2477.
32 M. Kaempgen, G. Duesberg and S. Roth, *Appl. Surf. Sci.*, 2005, **252**, 425-429.
33 B. Balamurugan, I. Aruna, B. R. Mehta and S. M. Shivaprasad, *Phys. Rev. B*, 2004, **69**, 165419.
34 G. Liu, Y. Zhao, K. Deng, Z. Liu, W. Chu, J. Chen, Y. Yang, K. Zheng, H. Huang and W. Ma, *Nano Lett.*, 2008, **8**, 1071-1075.
35 S. M. Chou, M. H. Hon, C. Leu and Y. H. Lee, *J. Electrochem. Soc.*, 2008, **155**, H923-H928.
36 L. F. Hu, J. Yan, M. Y. Liao, H. J. Xiang, X. G. Gong, L. D. Zhang and X. S. Fang, *Adv. Mater.*, 2012, **24**, 2305-2309.
37 Y. Lin, K. Zhang, W. Chen, Y. Liu, Z. Geng, J. Zeng, N. Pan, L. Yan, X. Wang and J. Hou, *ACS Nano*, 2010, **4**, 3033-3038.
38 J. Zhao, J. Han and J. P. Lu, *Phys. Rev. B*, 2002, **65**, 193401.
39 W. Su, T. Leung, B. Li and C. Chan, *Appl. Phys. Lett.*, 2007, **90**, 163103.
40 J. Liu, J. Park, K. H. Park, Y. Ahn, J. Y. Park, K. H. Koh and S. Lee, *Nanotechnology*, 2010, **21**, 485504.
41 Y. S. Lee, J. Heo, M. T. Winkler, S. C. Siah, S. B. Kim, R. G. Gordon and T. Buonassisi, *J. Mater. Chem. A*, 2013, **1**, 15416-15422.
42 C. X. Xiang, G. M. Kimball, R. L. Grimm, B. S. Brunschwig, H. A. Atwater and N. S. Lewis, *Energ. Environ. Sci.*, 2011, **4**, 1311-1318.
43 J. S. Kim, J. H. Park, J. H. Lee, J. Jo, D. Y. Kim and K. Cho, *Appl. Phys. Lett.*, 2007, **91**, 112111.
44 Z. Yu, A. Raman and S. Fan, *PNAS*, 2010, **107**, 17491-17496.
45 V. F. Drobny and D. L. Pulfrey, *Thin Solid Films*, 1979, **61**, 89-98.
46 X. W. Sun and H. S. Kwok, *J. Appl. Phys.*, 1999, **86**, 408-411.
47 L. F. Hu, M. Chen, W. Z. Shan, T. R. Zhan, M. Y. Liao, X. S. Fang, X. H. Hu and L. M. Wu, *Adv. Mater.*, 2012, **24**, 5872-5877.
48 Y. Yao, J. Yao, V. K. Narasimhan, Z. Ruan, C. Xie, S. Fan and Y. Cui, *Nature Commun.*, 2012, **3**, 664.

Figure Captions

Fig. 1. SEM images of (a and d) SWNTs-coated PET sheet, (b and e) ZnO/SWNTs hybrid nanofilms, and (c and f) Cu_2O/ZnO/SWNTs hybrid nanofilms at different magnifications. (g) Optical image of the flexible PET sheet with Cu_2O/ZnO hybrid nanofilms.

Fig. 2. The XRD patterns of (a) pristine PET sheet, (b) SWNTs-coated PET sheet, (c) ZnO/SWNTs hybrid nanofilms, and (d) Cu_2O/ZnO/SWNTs hybrid nanofilms.

Fig. 3. (a) Survey XPS spectrum, and (b-d) Cu 2p, Zn 2p and (d) O 1s core evel XPS spectra of the Cu_2O/ZnO/SWNTs hybrid nanofilms.

Fig. 4. (a) Schematic diagram illustrating the photodetector fabrication procedure of the Cu_2O/ZnO hybrid nanofilms on SWNTs-based PET. (b) I-V characteristics of the Cu_2O/ZnO photodetector with ITO/Cu_2O/ZnO/SWNTs structure under dark condition. (c) Time-resolved photoresponse of the device upon four monochromic LED lights without applied bias. The LED lights used here are UV (365 nm, 0.3 mW/cm^2), blue (425 nm, 3.2 mW/cm^2), green (525 nm, 6.9 mW/cm^2) and red (625 nm, 2.3 mW/cm^2). (d) Time-resolved photoresponse of the device upon different intensities of white LED lights without applied bias. (e) Enlarged portion of one photocurrent rising and reset under white LED illumination of 28.7 mW/cm^2.

Fig. 5. (a) Schematic diagram illustrating the photodetector fabrication procedure of the ZnO/Cu_2O hybrid nanofilms on SWNTs-based PET. (b) Time-resolved photoresponse of the device upon four monochromic LED lights without applied bias. The LED lights used here are UV (365 nm, 0.3 mW/cm^2), blue (425 nm, 3.2 mW/cm^2), green (525 nm, 6.9 mW/cm^2) and red (625 nm, 2.3 mW/cm^2). (c) Time-resolved photoresponse of the device upon different intensities of white LED lights without applied bias.

Fig. 6. Energy level diagrams with respect to vacuum level for the photodetectors with the structure of (a) ITO/Cu_2O/ZnO/SWNTs, and (b) ITO/ZnO/Cu_2O/SWNTs. (c) UV-vis absorption spectra of ZnO, Cu_2O, ZnO/Cu_2O and Cu_2O/ZnO nanofilms.

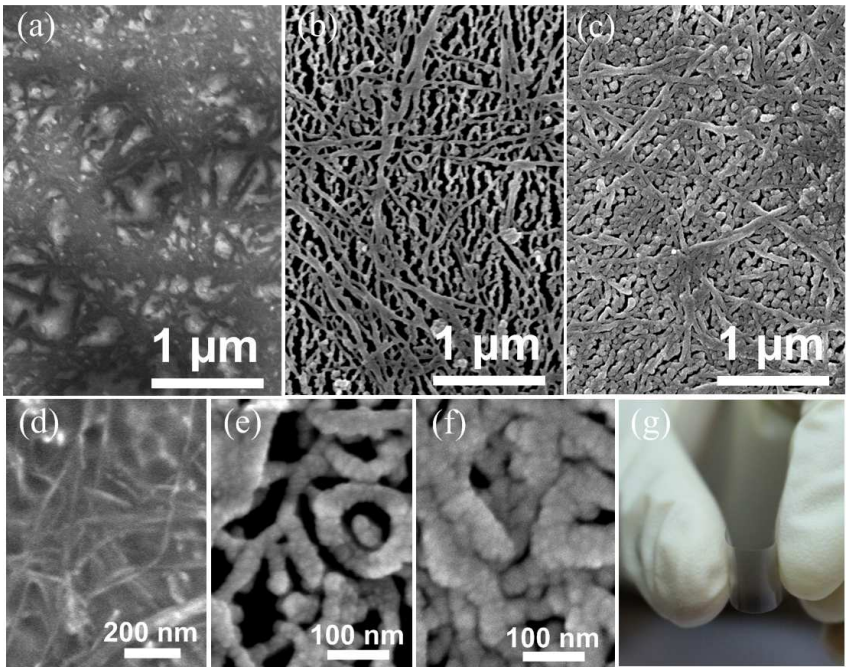

Fig. 1. SEM images of (a and d) SWNTs-coated PET sheet, (b and e) ZnO/SWNTs hybrid nanofilms, and (c and f) Cu_2O/ZnO/SWNTs hybrid nanofilms at different magnifications. (g) Optical image of the flexible PET sheet with Cu_2O/ZnO hybrid nanofilms.

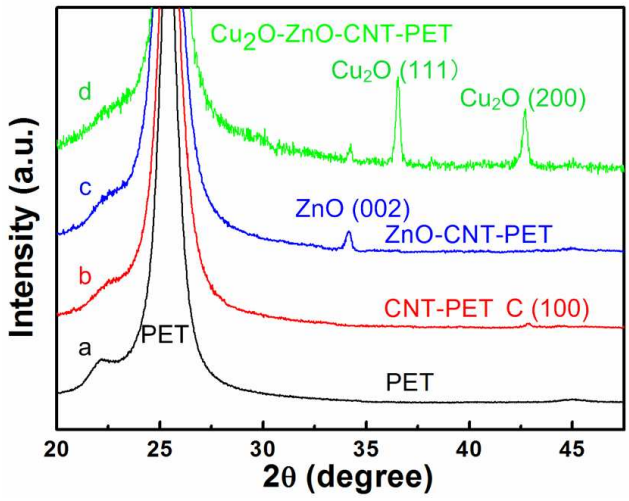

Fig. 2. The XRD patterns of (a) pristine PET sheet, (b) SWNTs-coated PET sheet, (c) ZnO/SWNTs hybrid nanofilms, and (d) Cu_2O/ZnO/SWNTs hybrid nanofilms.

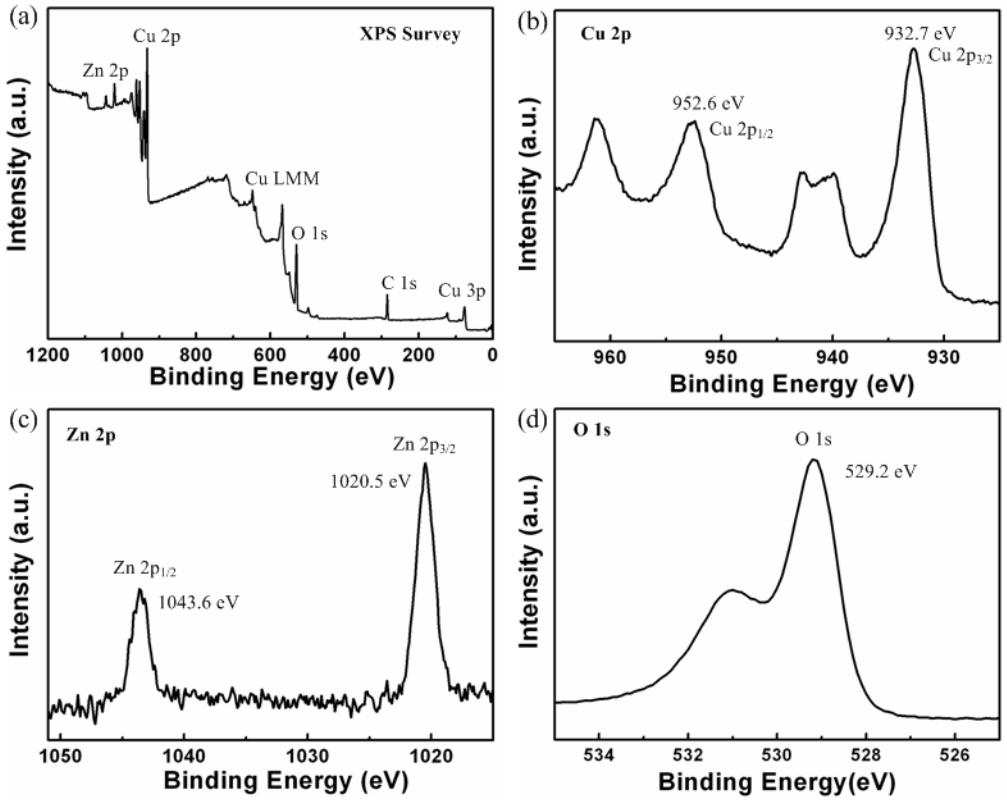

Fig. 3. (a) Survey XPS spectrum, and (b-d) Cu 2p, Zn 2p and (d) O 1s core evel XPS spectra of the Cu_2O/ZnO/SWNTs hybrid nanofilms.

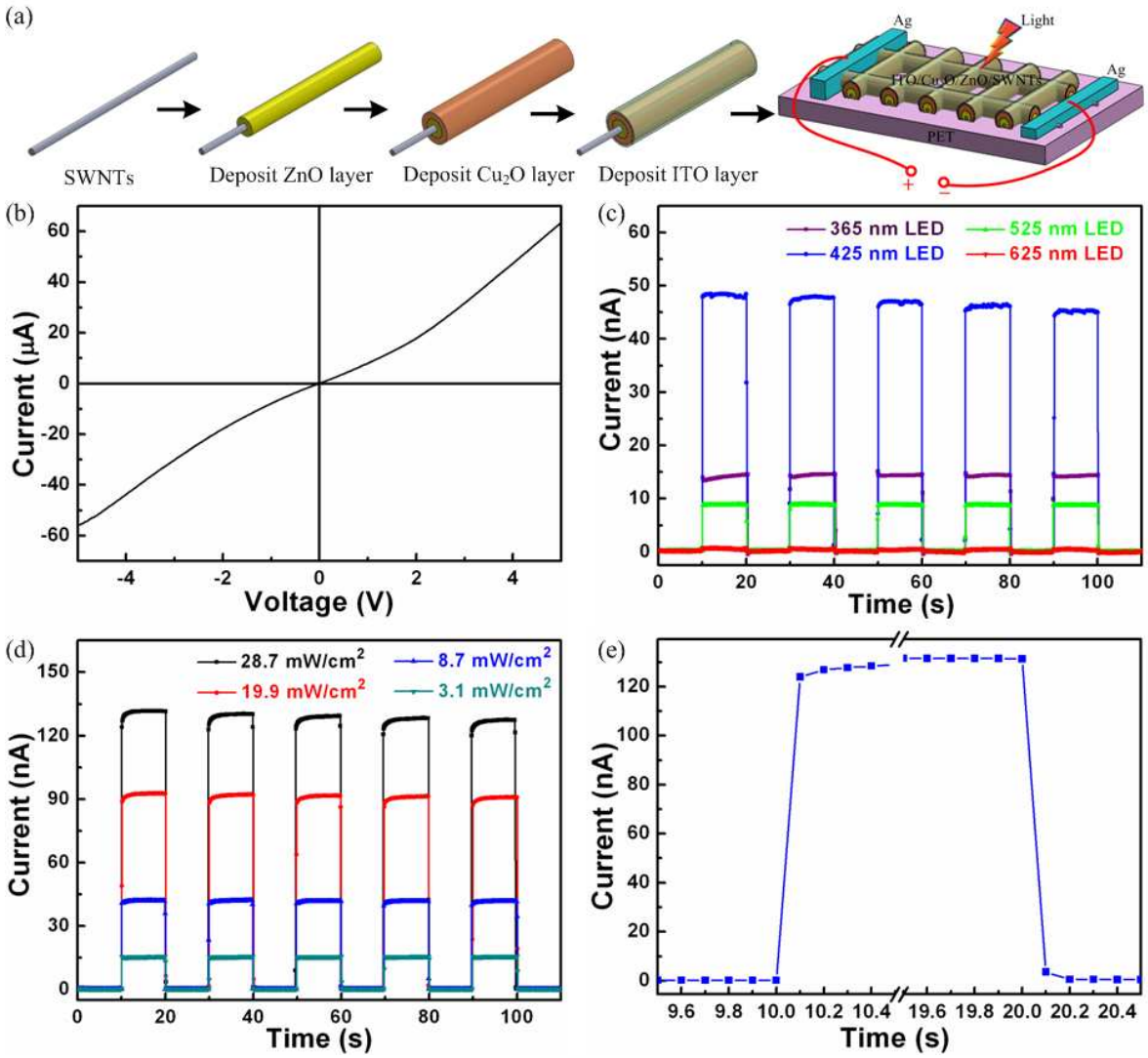

Fig. 4. (a) Schematic diagram illustrating the photodetector fabrication procedure of the Cu_2O/ZnO hybrid nanofilms on SWNTs-based PET. (b) I-V characteristics of the Cu_2O/ZnO photodetector with ITO/Cu_2O/ZnO/SWNTs structure under dark condition. (c) Time-resolved photoresponse of the device upon four monochromic LED lights without applied bias. The LED lights used here are UV (365 nm, 0.3 mW/cm^2), blue (425 nm, 3.2 mW/cm^2), green (525 nm, 6.9 mW/cm^2) and red (625 nm, 2.3 mW/cm^2). (d) Time-resolved photoresponse of the device upon different intensities of white LED lights without applied bias. (e) Enlarged portion of one photocurrent rising and reset under white LED illumination of 28.7 mW/cm^2.

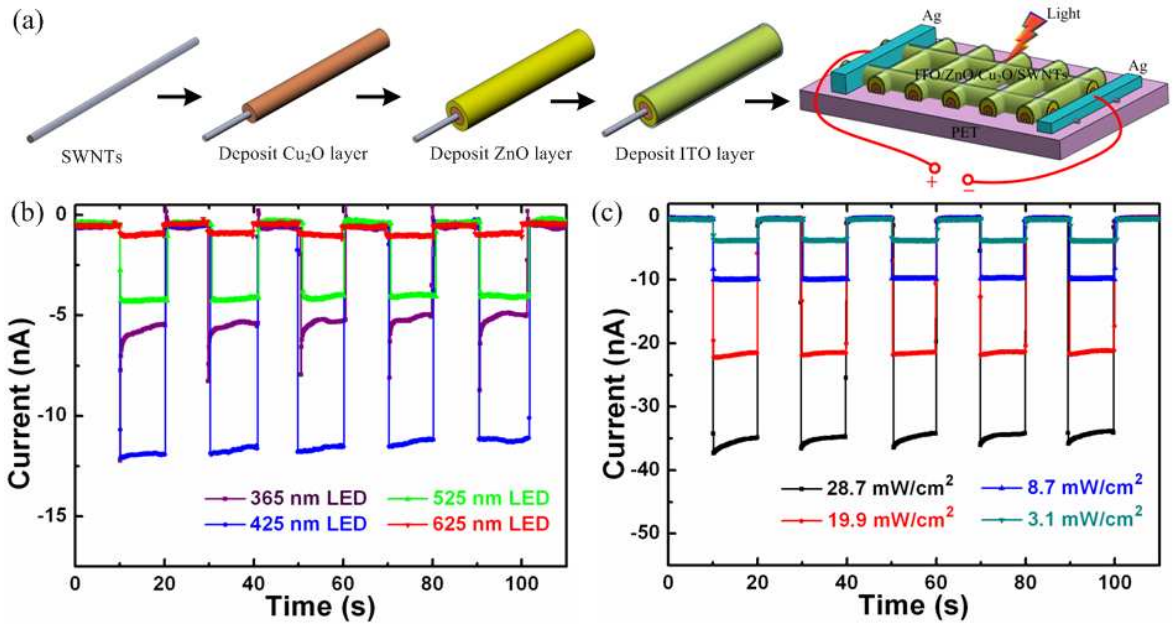

Fig. 5. (a) Schematic diagram illustrating the photodetector fabrication procedure of the ZnO/Cu_2O hybrid nanofilms on SWNTs-based PET. (b) Time-resolved photoresponse of the device upon four monochromic LED lights without applied bias. The LED lights used here are UV (365 nm, 0.3 mW/cm^2), blue (425 nm, 3.2 mW/cm^2), green (525 nm, 6.9 mW/cm^2) and red (625 nm, 2.3 mW/cm^2). (c) Time-resolved photoresponse of the device upon different intensities of white LED lights without applied bias.

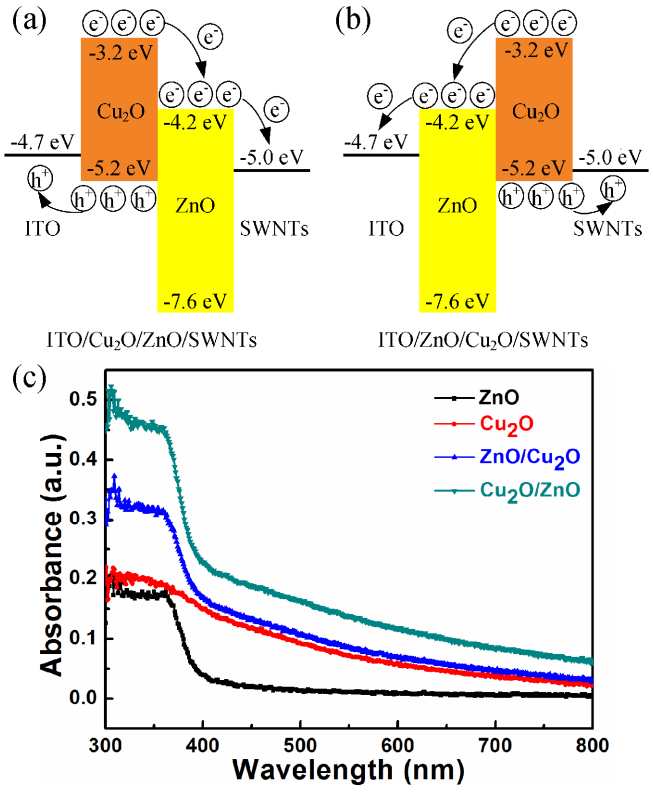

Fig. 6. Energy level diagrams with respect to vacuum level for the photodetectors with the structure of (a) ITO/Cu_2O/ZnO/SWNTs, and (b) ITO/ZnO/Cu_2O/SWNTs. (c) UV-vis absorption spectra of ZnO, Cu_2O, ZnO/Cu_2O and Cu_2O/ZnO nanofilms.